Near-field Experimental Verification of the EM Models for the LOFAR Radio Telescope

P. Bolli, G. Pupillo, F. Paonessa, G. Virone, *Member, IEEE*, S.J. Wijnholds, *Senior Member, IEEE*, and A.M. Lingua

Abstract—**Modern radio astronomical facilities in the VHF band consist of large antenna arrays with digital beamforming. The calibration of these instruments requires accurate models of their electromagnetic behavior. Numerical models covering the full telescope field-of-view are nowadays effectively computed by means of full-wave solvers. However, their experimental verification is still an open and challenging task. This letter proposes a verification strategy based on near-field scans. An Unmanned Aerial Vehicle carrying a test source is used to excite the array from a limited set of spatial points, located in the radiating near-field region. The collected data are directly used to verify the telescope electromagnetic model without additional post-processing. This exploits the capability of full-wave solvers to predict near-field patterns from the same geometrical and electrical model used to compute far-field patterns. The application of the proposed technique to the Low Frequency Array (LOFAR) radio telescope verified the predictions with residuals below 0.5 dB.**

Index Terms—**Antenna Measurements, Antenna Radiation Patterns, Near Fields, Phased Arrays, Radio Astronomy**

I. INTRODUCTION

THE continuous exponential increase of the performance of digital systems has impacted radio astronomy making phased array technology very popular either combined with traditional single-dish radio telescopes (known as phased array feeds) or as a radio observatory themselves (aperture arrays) [1]. For instance, the Low Frequency Array (LOFAR) instrument, developed by ASTRON, belongs to this latter category [2]. LOFAR has been developed as scientific and technological path-finder for the low-frequency instrument of the Square Kilometre Array (SKA) [3].

The instrumental calibration of aperture arrays requires, for every angular direction within the field-of-view, an accurate model of the far-field radiation pattern of each element. This includes taking into account the coupling effects with other antennas and with the surrounding environment. These models can be completely computed exploiting currently available full-wave solvers. However, the experimental validation of their accuracy level is not straightforward owing to both the large
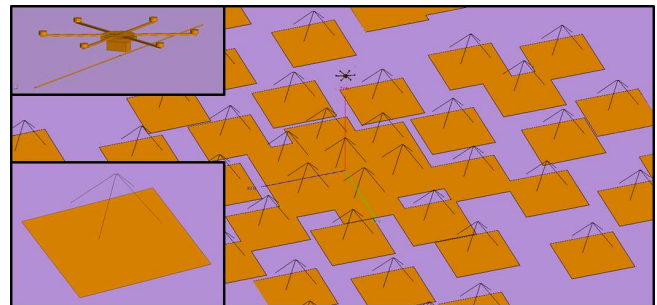

Fig. 1. Geometrical model of the LBA inner with the UAV. The UAV is shown at 5-m height from the array center for demonstration purpose. The insets on the left side show the UAV-mounted test source (top) and a single LBA (bottom).

size of the considered antenna arrays (more than 30 m) and the low operating frequency (down to 30 MHz).

Astronomical sources can only be adopted to perform partial far-field pattern verifications [4] due to their intrinsically limited spatial coverage. Moreover, a pre-calibrated beamforming system is required to achieve enough sensitivity. Crane-mounted sources [5] have enough power to operate at element level, without the required spatial coverage. Helicopter [6] and balloon-borne sources provide both enough power and spatial coverage at a high cost. Recently, the development of Unmanned Aerial Vehicle (UAV) technology allowed for a low-cost and efficient experimental characterization of single antenna elements [5]-[9], and small array prototypes [10],[11] in their far-field regime. In this contribution, the same system is used to perform the antenna verification with the UAV located in the near-field region.

Systems like LOFAR and the low-frequency telescope of the SKA consist of many antennas grouped in subarrays that are referred to as *stations*. Technical constraints and regulations define a maximum height for the UAV, which makes it extremely difficult to satisfy the far-field conditions for such stations, e.g. 270 m and 420 m for a 30-m station at 44 and 70 MHz, respectively. In order to deal with these limitations, a model verification strategy based on both measurements and simulations in the radiating near-field region of the array is

Manuscript submitted on XXXXX
P. Bolli is with the Istituto Nazionale di Astrofisica (INAF) - Osservatorio Astrofisico di Arcetri, Florence, Italy (e-mail: pbolli@arcetri.inaf.it).
G. Pupillo is with the Istituto Nazionale di Astrofisica (INAF) - Istituto di Radioastronomia, Bologna, Italy (e-mail: g.pupillo@ira.inaf.it).
G. Virone and F. Paonessa are with the Consiglio Nazionale delle Ricerche - Istituto di Elettronica e di Ingegneria dell'Informazione e delle

Telecomunicazioni (CNR-IEIIT), Turin, Italy (e-mail: giuseppe.virone@ieiit.cnr.it, fabio.paonessa@ieiit.cnr.it).
S.J. Wijnholds is with the Netherlands Institute for Radio Astronomy (ASTRON), Dwingeloo, The Netherlands (e-mail: wijnholds@astron.nl).
A.M. Lingua is with the Environment, Land and Infrastructure Department (DIATI) - Politecnico di Torino, Turin, Italy (e-mail: andrea.lingua@polito.it).

presented in this letter. This technique is independent of the adopted beamforming strategy. Results for the low-frequency (below 100 MHz) sub-system of a LOFAR station are reported as near-field beam patterns focused in two different spatial points.

II. NEAR-FIELD SCANS WITH THE UAV-MOUNTED TEST SOURCE

The UAV-mounted test source described in [10] can perform autonomous trajectories defined as arbitrary series of waypoints. During the flight, its position is measured using an on-board differential GNSS system with an uncertainty of about 2 cm in the horizontal plane and 7 cm in height. The UAV orientation is measured with its internal inertial measurement unit with an accuracy of ±2°. For this experiment, a 2-m long thin dipole resonating around 70 MHz was horizontally mounted on the UAV (see Fig. 1). Further technical details on the UAV system can be found in Section 2 of [9].

The Friis equation approach described in [7] and [10] is no longer valid in the near-field regime. In this case, a more general model in terms of the transmission coefficient $t_i(s)$ between the UAV source port and the i-th array element port is required, where s is the curvilinear abscissa along the trajectory of the test source.

The transmission coefficients $t_i(s)$ are related to both the source and the array element radiation characteristics as well as their relative position. In particular, in the near-field region, all the elements see the source at a different angle (parallax effect).

From the experimental side, the transmission coefficients $t_i(s)$ are measured with the telescope recording system during the UAV flight. They are proportional to the acquired complex voltages. However, a common unknown phase term is present since the test source is not phase-locked to the receiver. As well known, this feature prevents the possibility of performing a canonical near-field to far-field transformation. On the other hand, phaseless transformation techniques [12] will require a large number of dense linear trajectories over the array (multiple raster scans).

On the contrary, in commercial full-wave solvers, the near-field simulation of the $t_i(s)$ can be performed on the same model that is used to predict the far-field patterns. This feature suggested the near-field array model verification that is described in this letter. A similar approach has been presented in [13] for an array of two antennas, where the far-field condition was satisfied at the element level.

The high signal-to-noise ratio of the acquired complex voltages (proportional to $t_i(s)$) would not require any array beamforming strategy, i.e., the model validation could be done at the element level. However, owing to the large number of elements in a station (46 or more for LOFAR, 256 for SKA), it is convenient to present the data in an aggregated form. A normalized array transmission coefficient is defined by combining the $t_i(s)$ of all the antennas according to the following formula

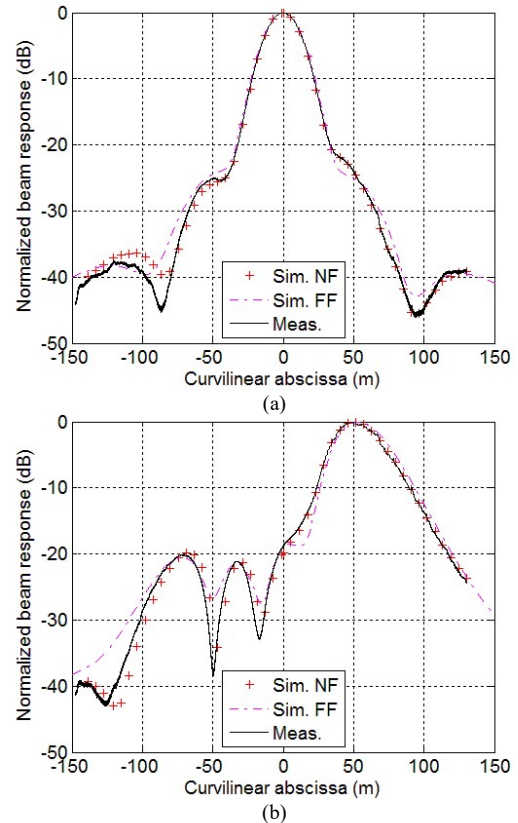$$T(s) = \frac{1}{N}\sum_{i=1}^{N} t_i(s)/t_i(s_0) \qquad (1)$$

Fig. 2. Normalized transmission coefficient of LBA inner at 44 MHz and 100-m height: measurements (black line), near-field simulations (red crosses) and far-field simulations (magenta dashed line). Focused: (a) at 0°, (b) at 30°.

where N is the number of elements. All the contributions are equalized at s_0 forming a maximum in this point. This choice produces very focused beams, with higher dynamic range with respect to the element patterns, in order to reveal the smaller discrepancies.

III. LOFAR EM MODEL VERIFICATION

The LOFAR radio telescope is an aperture synthesis array composed of phased array stations. Each station includes two different receiving systems: a random sparse array of Low Band Antennas (LBA) and the High Band Antenna tiles, operating in the frequency bands 30 – 80 MHz and 120 – 240 MHz, respectively [2]. The LBA consists of two orthogonal inverted-V dipole antennas above a mesh ground plane of 3 m x 3 m (see Fig. 1). Each LOFAR core station includes 96 LBAs irregularly distributed around a central point and aligned towards either North-East (NE) or South-West directions. The LOFAR system simultaneously acquires data from either 46 antennas located within a radius of about 30 m plus 2 outer antennas for calibration (identified as LBA inner) or the external 48 antennas spread within a circle with radius of about 85 m (LBA outer). The analysis and the results presented in this letter refer to the central 46 antennas of the LBA inner only. Both the LBA inner array and the UAV system have been simulated using the commercial antenna software package FEKO. The method of moments implemented in FEKO performs a full-wave analysis of the model including the dielectric terrain (assumed to have a relative permittivity of 3)
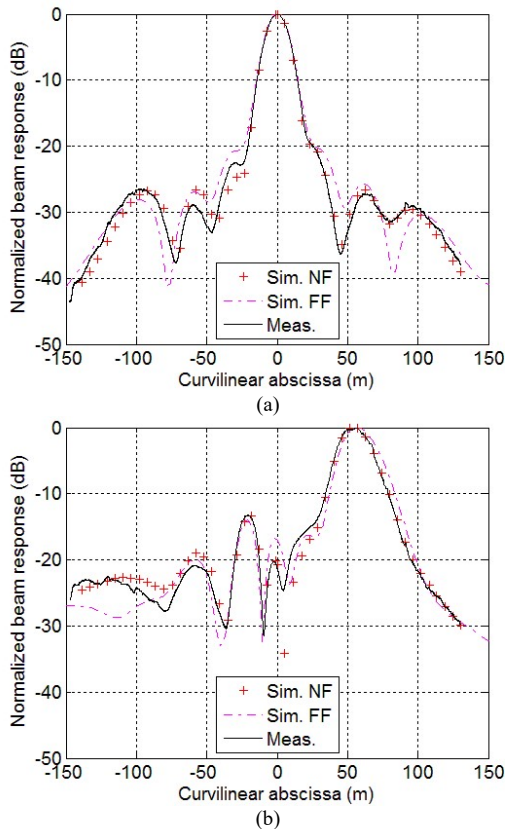
Fig. 3. Normalized transmission coefficient of LBA inner at 70 MHz and 100-m height: measurements (black line), near-field simulations (red crosses) and far-field simulations (magenta dashed line). Focused: (a) at 0°, (b) at 30°.
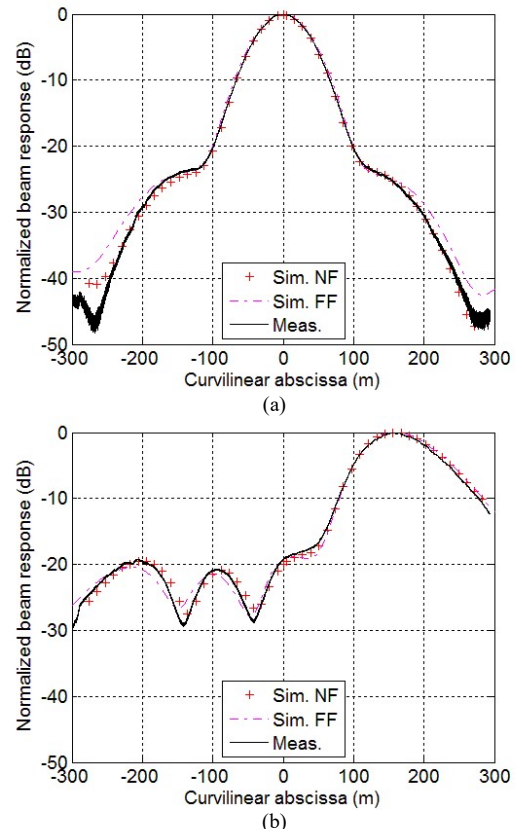

Fig. 4. Normalized transmission coefficient of LBA inner at 44 MHz and 300-m height: measurements (black line), near-field simulations (red crosses) and far-field simulations (magenta dashed line). Focused: (a) at 0°, (b) at 30°.

and the coupling between elements. Scattering parameter lumped ports are used for both the elements and the source.

In the following, an example of the LOFAR model verification is presented exploiting two linear flights at constant height (100 and 300 m) in the E-plane of the LBA inner. For both heights, the total length of the trajectory is chosen so that the field-of-view of the LBA (about 45 degrees) is covered. The real trajectory of the UAV was decimated to 50 points. For each of them, a run in FEKO was performed by using the measured UAV position and orientation. Each run produces all transmission coefficients t_i from the electrical port of the source to the LBA ports, considering a reference impedance of 50 Ω.

Figs. 2 to 5 show the normalized array transmission coefficient as given by (1), where the coefficients t_i have been both measured and simulated. The array transmission coefficient is focused on two different points s_0: one above the central element (0°, zenith direction at the array center) and one about 30° off from the zenith direction. Moreover, the analysis has been conducted for two different frequencies: 44 and 70 MHz. As far as the measured results are concerned, both frequencies were acquired simultaneously owing to the processing power of the LOFAR digital backend. In particular, higher-order harmonics of the RF synthesizer were exploited [14].

For the 100-m altitude flight, the normalized array near-field transmission coefficients at 44 and 70 MHz are shown in Figs. 2

and 3, respectively. The 300-m altitude case is shown in Figs. 4 and 5. In all cases, the agreement in the main lobe between near-field simulations and measured data is very remarkable. For the secondary lobes, there is a general agreement although with a larger discrepancy.

The normalized transmission coefficient has been also computed using the Friis transmission equation approach in [7], based on the embedded-element far-field patterns, the UAV source pattern and the free-space path-loss. As evident from Figs. 2 to 5, the far-field approach is also quite accurate although higher discrepancies are present.

A quantitative figure of merit for the difference between measured and simulated data has been calculated using the weighted logarithmic difference introduced in equation (7) of [15] with the exponential coefficient of weights (β) equal to 0.5. These differences are plotted in Fig. 6 (focus at 0°). For both frequencies and heights, there is a significant improvement in the comparison by using the near-field simulations (within ±0.5 dB) with respect to the far-field ones (more than 1 dB at 70 MHz). This highlights the importance of the adopted near-field full-wave approach to the telescope model verification.

The measurement accuracy in the UAV position and orientation (see [9]) is negligible with respect to the achieved residuals. Therefore, the latter are entirely related to the model and manufacturing uncertainties of both the array and the test source.
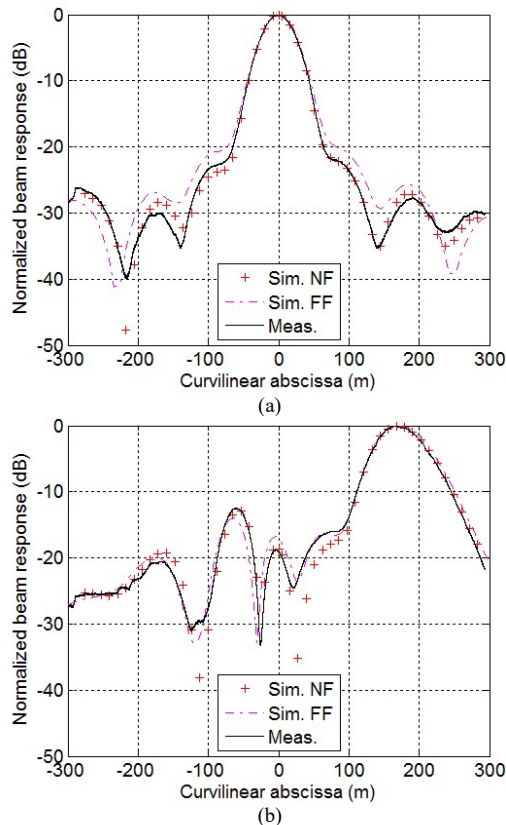
(a)

(b)

Fig. 5. Normalized transmission coefficient of LBA inner at 70 MHz and 300-m height: measurements (black line), near-field simulations (red crosses) and far-field simulations (magenta dashed line). Focused: (a) at 0°, (b) at 30°.
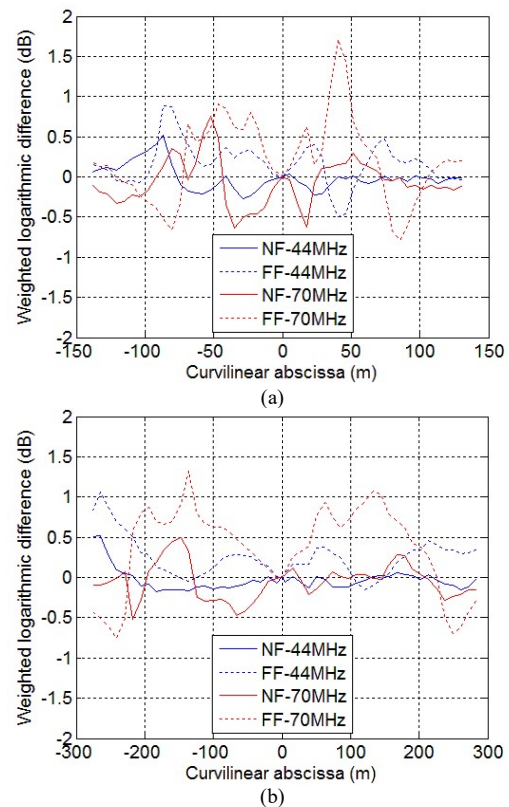

(a)

(b)

Fig. 6. Weighted logarithmic difference for near-field (solid lines) and far-field (dotted lines) simulations compared to the measurements (focus at 0°) and frequencies 44 (blue lines) and 70 MHz (red lines). Heights: (a) 100 m, (b) 300 m.

IV. CONCLUSIONS

UAV-mounted test sources are a convenient tool for in-situ performance assessment and model validation of radio astronomical phased arrays. Such measurements need to be performed in the radiating near-field region due to the large size of these antenna systems. This particular operating condition of the test source has been exploited to validate the telescope electromagnetic models. The comparison between experimental and predicted data for a LOFAR LBA station demonstrates residuals below 0.5 dB.

REFERENCES

[1] A. van Ardenne, et al., "Extending the Field of View With Phased Array Techniques: Results of European SKA Research," *Proceedings of the IEEE*, 97, (8), pp. 1531–1542, 2009.

[2] M.P. van Haarlem, et al., "LOFAR: The Low Frequency Array," *Astronomy & Astrophysics*, 556, (A2), pp. 1–53, 2013.

[3] M.G. Labate, et al., "The SKA low-frequency telescope: Performance parameters and constraints on the array configuration," *11th European Conference on Antennas and Propagation*, pp. 2259–2263, 2017.

[4] A.T. Sutinjo, et al., "Characterization of a Low-Frequency Radio Astronomy Prototype Array in Western Australia," *IEEE Trans. on Antennas Propag.*, 63, (12), Dec. 2015.

[5] A. Nelles, et al., "Calibrating the absolute amplitude scale for air showers measured at LOFAR," *Journal of Instrumentation*, 10, (11), 2015.

[6] B. Witvliet, "Airborne evaluation/verification of antenna patterns of broadcasting stations," *18th International Wroclaw Symposium and Exhibition on Electromagnetic Compatibility*, Wroclaw, June, 2006.

[7] G. Virone, et al., "Antenna Pattern Verification System Based on a Micro Unmanned Aerial Vehicle (UAV)," *IEEE Antennas and Wireless Propagation Letters*, 13, pp. 169–172, 2014.

[8] D.C. Jacobs, et al., "First Demonstration of ECHO: an External Calibrator for Hydrogen Observatories," *Publications of the Astronomical Society of the Pacific*, 129:035002, Mar. 2017.

[9] P. Bolli, et al., "Antenna pattern characterization of the low-frequency receptor of LOFAR by means of an UAV-mounted artificial test source," in *Proceedings SPIE - Ground-based and Airborne Telescopes VI*, 9906, July 2016.

[10] G. Pupillo, et al., "Medicina array demonstrator: calibration and radiation pattern characterization using a UAV-mounted radio-frequency source," *Experimental Astronomy*, 39, (2), pp. 405–421, 2015.

[11] E. de Lera Acedo, et al., "SKA Aperture Array Verification System: Electromagnetic modeling and beam pattern measurements using a micro UAV," *Experimental Astronomy,* in press.

[12] M.G. Fernandez, et al., "Antenna Diagnostics and Characterization using Unmanned Aerial Vehicles," *IEEE Access*, DOI: 10.1109/ACCESS.2017.2754985.

[13] N. Stangl, "MF AM Antenna Radiation Pattern Verification Method by Near Field Measurements," *IEEE Transactions on Broadcastings*, 47, (3), Sept. 2001.

[14] P. Bolli, et al., "In-Situ Characterization of International Low-Frequency Aperture Arrays by Means of an UAV-based System", *32nd URSI GASS*, Montreal, August 2017.

[15] S. Pivnenko, et al., "Comparison of Antenna Measurement Facilities With the DTU-ESA 12 GHz Validation Standard Antenna Within the EU Antenna Centre of Excellence," *IEEE Trans. Antennas Propagat.*, 57, (7) pp. 1873–1878, 2009.